International Journal of Mechanical System Dynamics

WILEY

IJMSD International Journal of Mechanical System Dynamics Open Access

RESEARCH ARTICLE OPEN ACCESS

Three Benefits of Using Nonlinear Compliance in Robotic Systems Performing Cyclic Tasks: Energy Efficiency, Control Robustness, and Gait Optimality

Rezvan Nasiri[1,2,3] | Mahdi Khoramshahi[4] | Mohammad Javad Yazdanpanah[3,5] | Majid Nili Ahmadabadi[1,2,3]

[1]Cognitive Systems Laboratory, University of Tehran, Tehran, Iran | [2]Research Institute for Robotic Artificial Intelligence and Information Science Control (RAIIS), University of Tehran, Tehran, Iran | [3]Control and Intelligent Processing Center of Excellence (CIPCE), School of Electrical and Computer Engineering, College of Engineering, University of Tehran, Tehran, Iran | [4]ISIR, Sorbonne University, Paris, France | [5]Advanced Control Systems, University of Tehran, Tehran, Iran

Correspondence: Rezvan Nasiri (rezvan.nasiri@ut.ac.ir)

Received: 29 December 2024 | **Revised:** 5 March 2025 | **Accepted:** 14 March 2025

Keywords: control robustness | cyclic tasks | energy efficiency | gait optimality | nonlinear compliance

ABSTRACT

Nonlinearity in parallel compliance can be exploited to improve the performance of locomotion systems in terms of (1) energy efficiency, (2) control robustness, and (3) gait optimality; that is, attaining energy efficiency across a set of motions. Thus far, the literature has investigated and validated only the first two benefits. In this study, we present a new mathematical framework for designing nonlinear compliances in cyclic tasks encompassing all three benefits. We present an optimization-based formulation for each benefit to obtain the desired compliance profile. Furthermore, we analytically prove that, compared to linear compliance, using nonlinear compliance leads to (1) lower energy consumption, (2) better closed-loop performance, specifically in terms of tracking error, and (3) a higher diversity of natural frequencies. To compare the performance of linear and nonlinear compliance, we apply the proposed methods to a diverse set of robotic systems performing cyclic tasks, including a 2-DOF manipulator, a 3-DOF bipedal walker, and a hopper model. Compared to linear compliance, the nonlinear compliance leads to better performance in all aspects; for example, a 70% reduction in energy consumption and tracking error for the manipulator simulation. Regarding gait optimality, for all robotic simulation models, compared to linear compliance, the nonlinear compliance has lower energy consumption and tracking error over the considered set of motions. The proposed analytical studies and simulation results strongly support the idea that using nonlinear compliance significantly improves robotic system performance in terms of energy efficiency, control robustness, and gait optimality.

1 | Introduction

Nature has been the source of many inspirations in the robotic field. For some instances, we can refer to central pattern generators (CPGs) to generate cyclic motions for robotic systems [1], vision-inspired camera feedback for path planning [2], and push-off actuation for legged robots inspired by the human reflex mechanism in walking [3]. Since Alexander introduced the three benefits of compliance (i.e., the pogo stick principle, return spring, and foot pad) in legged locomotion in 1990 [4], many designers have incorporated compliance into their robotic systems to enhance robot performance in terms of force control [5], stability [6], joint synchrony [7], safety [8], and energy efficiency [9, 10]. In the recent decade, robotic researchers have tried to present systemic frameworks for the design of compliant joints [11–13] and bodies [14–16].

Compliance appears in two main configurations in robotic joints: parallel or serial [17–20]. Although both configurations are beneficial, due to the additive relation of the actuator and parallel compliance forces, parallel compliance provides a

well-posed mathematical framework for actuator force compensation and consequently energy consumption reduction. In other words, parallel compliance attains *energy efficiency* by actuator force reduction, which also minimizes actuator size and weight. This cannot be achieved by other energy-saving approaches such as regenerative braking or supercapacitors. Here, we focus only on the benefits of using parallel compliance, and whenever we refer to compliance, it is only parallel compliance.

From a dynamical perspective, adding proper nonlinear compliance modifies the robot's natural dynamics toward the desired dynamics; that is, natural dynamics modification [21]. In other words, parallel compliance modifies the natural dynamics such that the system does not require complex control systems [22], and a weak and simple controller (e.g., a PD controller with limited actuation force) traces the desired trajectory with lower energy consumption and higher *control robustness* [13]. From a practical view, compliance as a physical entity has much higher bandwidth and functional safety compared to any implemented controller on digital hardware; that is, the digital controller has a limited updating rate and failure risk. In our previous work [23], we showed that the design of nonlinear compliance enhances closed-loop performance such that impulsive and discontinuous actuations can properly trace the reference trajectory both in cyclic and explosive tasks.

From another perspective, legged animals utilize the coupling between frequency and amplitude of motions (i.e., gait; see Figure 1) provided by their compliant body to attain stability in different environments [24] and maintain efficiency and robustness in extreme conditions. We call this property *gait optimality*, which is first introduced in [25]. Accordingly, the body dynamics/compliance should be optimized across the gait (i.e., a set of motions) rather than a specific motion [26–28]. Inspired by this biological fact, for the first time, we present an optimization framework to design nonlinear compliance to enhance gait optimality. Instead of having a single "natural" frequency in linear compliances, nonlinear compliances allow for coupling between "natural" frequency and amplitude. In other words, motions with different frequencies can be "natural" if we utilize their corresponding amplitude; that is, *frequency-amplitude coupling* (FAC).

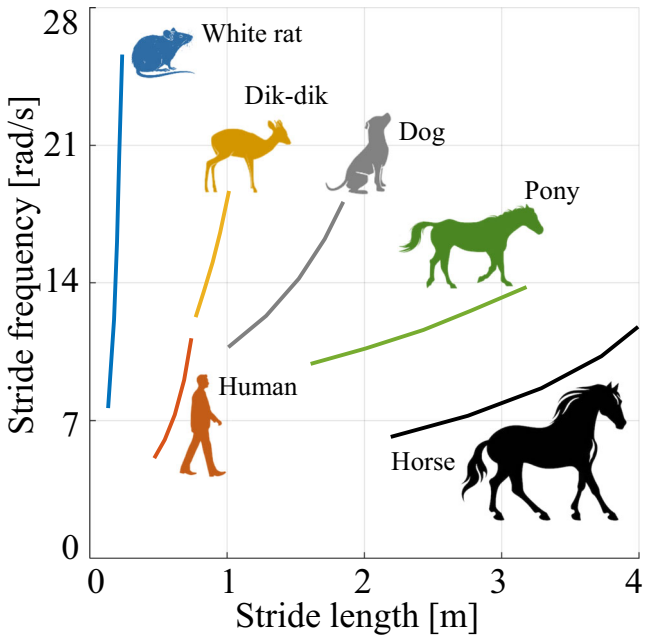

FIGURE 1 | The gait frequency as a function of stride length in humans and animals [29–31]. This figure provides evidence for frequency-amplitude coupling (FAC) in biological systems. Also, this figure suggests that the FAC function for almost all of the presented biological systems is monotonically increasing, indicating that they all benefit from similar locomotion principles/dynamics. The animal and human images are from [32].

Regardless of the mentioned superiority of nonlinear compliance over linear compliance in different aspects, to the best of our knowledge, there is still no general mathematical framework for the design of nonlinear compliance to improve energy efficiency, control robustness, and gait optimality in cyclic tasks. Hence, in this paper, we analytically prove that, compared to linear compliance, nonlinear compliance has lower energy consumption, better control robustness, and diverse frequency-amplitude coupling. In addition, we present a general mathematical framework for nonlinear compliance design to enhance energy efficiency, control robustness, and gait optimality. The paper is organized as follows. In Section 2, we present our analytical framework to optimize the compliance profile for (1) energy efficiency, (2) control robustness, and (3) gait optimality. The simulation results are presented in Section 3, where we compare '*no compliant*', '*linear compliance*', '*piecewise linear compliance*', and '*nonlinear compliance*' conditions in terms of energy consumption, tracking error, applied force, and gait optimality. Finally, the conclusions and discussions are presented in Section 4.

2 | Mathematical Analysis

Consider the block diagram of an n-DOF robotic system performing cyclic tasks as described in Figure 2. In this block diagram, $\boldsymbol{q}_d \in \mathbb{R}^n$ is the vector of T-periodic desired trajectories, $\boldsymbol{q} \in \mathbb{R}^n$ is the vector of real joint positions, $\boldsymbol{e} = \boldsymbol{q}_d - \boldsymbol{q}$ is the vector of tracking error, $\boldsymbol{F}_a \in \mathbb{R}^n$ is the vector of applied force by the controller and actuation system, and $\boldsymbol{F}_c \in \mathbb{R}^n$ is the vector of parallel compliance force at each joint. Accordingly, the dynamical equations of the system can be written as:

$$H(\boldsymbol{q}, \dot{\boldsymbol{q}}, \ddot{\boldsymbol{q}}) = \boldsymbol{F}_a - \boldsymbol{F}_c \; ; \; H: \; \mathbb{R}^n \times \mathbb{R}^n \times \mathbb{R}^n \to \mathbb{R}^n, \qquad (1)$$

where H represents the robot nonlinear dynamical equations that map the robot joint positions ($\boldsymbol{q}$), velocities ($\dot{\boldsymbol{q}}$), and

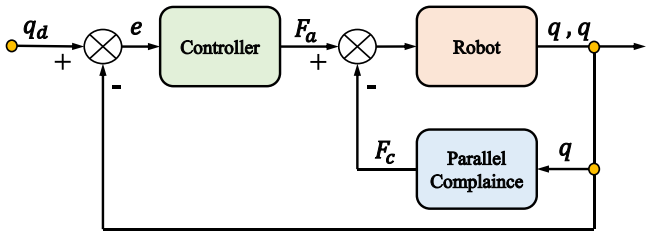

FIGURE 2 | Control block diagram of a robotic system with nonlinear parallel compliance at each joint. Note that all of the parameters are vectors.

accelerations ($\ddot{\boldsymbol{q}}$) to the applied force ($\boldsymbol{F}_a$) at the joint level. $\boldsymbol{F}_{cj}$ is the parallel compliance force[1] at the j^{th} joint, which is a function of the joint position (q_j).

Definition 1 (Compliance force). To parameterize the compliance force, we define it as a weighted sum of m nonlinear, sufficiently smooth, bounded, and persistently exciting basis functions ($\boldsymbol{\Phi}$) of the joint position ($\boldsymbol{q}$) as follows:

$$F_c(q) \triangleq \boldsymbol{K}^{\mathrm{T}}\boldsymbol{\Phi}(q)\ ;\ \boldsymbol{K}, \boldsymbol{\Phi} \in \mathbb{R}^m. \tag{2}$$

In this formulation, the design of the compliance force profile ($F_c(q)$) is left to the computation of the basis coefficients ($\boldsymbol{K}$).

Definition 2 (Required force). The required force ($\boldsymbol{F}_r$) for the controller to track the desired trajectory (i.e., $\boldsymbol{q}_d \equiv \boldsymbol{q}$) is computed by replacing the desired trajectory into the dynamical equations as $\boldsymbol{F}_r \triangleq H(\boldsymbol{q}_d, \dot{\boldsymbol{q}}_d, \ddot{\boldsymbol{q}}_d)$. Accordingly, based on Equation (1), we have:

$$\boldsymbol{F}_r + \boldsymbol{F}_e = \boldsymbol{F}_a - \boldsymbol{F}_c \rightarrow \boldsymbol{F}_a = \boldsymbol{F}_r + \boldsymbol{F}_e + \boldsymbol{F}_c \tag{3}$$

where $\boldsymbol{F}_e \triangleq H(\boldsymbol{q}, \dot{\boldsymbol{q}}, \ddot{\boldsymbol{q}}) - H(\boldsymbol{q}_d, \dot{\boldsymbol{q}}_d, \ddot{\boldsymbol{q}}_d)$ is the vector of error force, which is due to the controller imperfection; in the perfect tracking case, we have $\boldsymbol{q}_d \equiv \boldsymbol{q}$ and $\boldsymbol{F}_e \equiv 0$.

Assumption 1 (Controller performance). It is assumed that the controller, without parallel compliance ($\boldsymbol{F}_c \equiv 0$), can guarantee a bounded and sufficiently small tracking error with an upper bound of $\gamma_e \in \mathbb{R}^+$; i.e., $\|\boldsymbol{e}\|_\infty \leq \gamma_e \ll \|\boldsymbol{q}_d\|_\infty$.

Using Assumption 1, we have $\boldsymbol{q}_d \cong \boldsymbol{q}$, and consequently, an approximately zero error force ($\boldsymbol{F}_e \cong 0$). Therefore, we can rewrite Equation (3) as $\boldsymbol{F}_a \cong \boldsymbol{F}_r + \boldsymbol{F}_c \rightarrow F_a \cong F_r + F_c$.

2.1 | Energy Efficiency

Since the compliance force is in an additive relation to the controller applied force, it can compensate the conservative portion of the applied force. Assuming the actuator cannot recycle the negative power, compensation of the applied force leads to energy consumption reduction. To design the nonlinear compliance for energy consumption reduction, we present the following cost function, which is the integral of the squared mechanical power ($F_a\dot{q}$) over one cycle.

$$J_E = \int_T F_a^2\dot{q}^2\mathrm{d}t. \tag{4}$$

In this equation, T is the period of one cycle such that $F_a(t \pm T) = F_a(t)$ and $q(t \pm T) = q(t)$. To compute the optimal compliance coefficients, we replace $\boldsymbol{F}_a = \boldsymbol{K}^{\mathrm{T}}\boldsymbol{\Phi} + \boldsymbol{F}_r$, calculate the partial derivative of J_E with respect to K, and compute K_E that minimizes J_E as follows:

$$K_E = -\boldsymbol{\Lambda}_E^{-1}\int_T \boldsymbol{F}_r\boldsymbol{\Phi}\dot{q}^2\mathrm{d}t,\ \Lambda_E = \int_T \boldsymbol{\Phi}^{\mathrm{T}}\boldsymbol{\Phi}\dot{q}^2\mathrm{d}t \in \mathbb{R}^{m\times m}. \tag{5}$$

Theorem 1 (Energy efficiency). *Using Equations (2) and (5), having a set of both linear and nonlinear bases in $\boldsymbol{\Phi}$ leads to nonlinear compliance, which has more potential to reduce energy consumption compared to linear compliance.*

Proof. We assume two basis functions (ϕ_1, ϕ_2), where the first basis function is linear ($\phi_1 = q$) and the second one (ϕ_2) is an arbitrary nonlinear and orthogonal[2] to the first one; that is, $\int_T \phi_1\phi_2\dot{q}^2\mathrm{d}t = 0$. Accordingly, we can compare the suggested cost function (J_E) in two different cases: (1) design of linear parallel compliance ($\Phi = \phi_1$ and $K = k_1$), and (2) design of nonlinear parallel compliance ($\boldsymbol{\Phi} = [\phi_1; \phi_2]$ and $\boldsymbol{K} = [k_1; k_2]$). Hence, we replace $\boldsymbol{F}_a = \boldsymbol{K}^{\mathrm{T}}\boldsymbol{\Phi} + \boldsymbol{F}_r$ and rewrite J_E in each case as follows:

$$J_{E1} = \int_T F_r^2\dot{q}^2\mathrm{d}t + k_1^2\int_T \phi_1^2\dot{q}^2\mathrm{d}t + 2k_1\int_T F_r\phi_1\dot{q}^2\mathrm{d}t \tag{6}$$

$$\begin{aligned} J_{E2} = &\int_T F_r^2\dot{q}^2\mathrm{d}t + k_1^2\int_T \phi_1^2\dot{q}^2\mathrm{d}t + k_2^2\int_T \phi_2^2\dot{q}^2\mathrm{d}t \\ &+ 2k_1\int_T F_r\phi_1\dot{q}^2\mathrm{d}t + 2k_2\int_T F_r\phi_2\dot{q}^2\mathrm{d}t \\ &+ 2k_1k_2\int_T \phi_1\phi_2\dot{q}^2\mathrm{d}t \end{aligned}. \tag{7}$$

In these equations, J_{E1} and J_{E2} are the corresponding cost functions for the linear and nonlinear cases, respectively. In J_{E2}, due to the orthogonality of the bases, the last term is zero. To show that nonlinear compliance has more potential to reduce energy consumption compared to linear compliance, it is sufficient to show $J_{E2} \leq J_{E1}$ or $\Delta J_E = J_{E2} - J_{E1} \leq 0$. Hence, computing ΔJ_E using Equation (5), we have:

$$\Delta J_E = k_2^2\int_T \phi_2^2\dot{q}^2\mathrm{d}t + 2k_2\int_T F_r\phi_2\dot{q}^2\mathrm{d}t = -k_2^2\int_T \phi_2^2\dot{q}^2\mathrm{d}t \leq 0. \tag{8}$$

According to this result, nonlinear compliance is always better than or equal to linear compliance for energy consumption reduction. This proof can also be derived for the cost functions in the next subsections. □

2.2 | Control Robustness

According to Figure 2, parallel compliance can be considered a nonlinear position-dependent controller. Hence, it can improve closed-loop control performance in the presence of an imperfect controller. In addition, parallel compliance has a mechanical realization in practice; thus, if the main controller fails (e.g., due to power shutdown), parallel compliance can preserve closed-loop stability. To achieve this goal, we maximize reliance on the compliance force by minimizing the control effort. Accordingly, we present the following cost function, which is the integral of the square of the controller's applied force over a cycle.

$$J_R = \int_T F_a^2\mathrm{d}t. \tag{9}$$

Analytically, the energy consumption cost suggested in Equation (4) is the weighted version of the robustness cost function in

Equation (9). Thus, the optimal coefficients that minimize the robustness cost function also reduce energy consumption.

To compute the optimal compliance coefficients, we replace $\boldsymbol{F}_a = \boldsymbol{K}^{\mathrm{T}}\boldsymbol{\Phi} + \boldsymbol{F}_r$, calculate the partial derivative of J_R with respect to K, and compute K_R that minimizes J_R as follows:

$$K_R = -\boldsymbol{\Lambda}_R^{-1}\int_T \boldsymbol{F}_r\boldsymbol{\Phi}\mathrm{d}t,\ \boldsymbol{\Lambda}_R = \int_T \boldsymbol{\Phi}^{\mathrm{T}}\boldsymbol{\Phi}\mathrm{d}t \in \mathbb{R}^{m\times m}. \tag{10}$$

In classical control, Equation (9) is a special form of the cost function suggested for designing the H_2 robust controller [34]. Accordingly, designing parallel compliance to minimize this cost function improves closed-loop robustness.

Theorem 2 (Control robustness). *For a PD controller, minimization of J_R in Equation (9) and tracking error minimization are equivalent.*

Proof. For PD controllers, we have $F_a = K_p e + K_d\dot{e}$; the cost function is computed as follows:

$$J_R = \int_T F_a^2\mathrm{d}t = \int_T K_p^2 e^2\mathrm{d}t + \int_T K_d^2\dot{e}^2\mathrm{d}t + 2K_pK_d\int_T e\dot{e}\mathrm{d}t. \tag{11}$$

If the tracking error is periodic ($e(t) = e(t \pm T)$), then $2\int_T e\dot{e}\mathrm{d}t = e^2(t) - e^2(t-T) = 0$, and we have:

$$J_R = \int_T F_a^2\mathrm{d}t = K_p^2\int_T e^2\mathrm{d}t + K_d^2\int_T \dot{e}^2\mathrm{d}t. \tag{12}$$

According to the resultant cost function, in PD controllers, the minimization of J_R is equivalent to the minimization of the tracking error and its time derivative. □

2.3 | Gait Optimality

Theorem 3 (Frequency-amplitude coupling). *In linear compliance, the "natural" frequency of oscillations is independent of the amplitude, while in nonlinear compliances, the natural frequency is a function of amplitude.*

Proof. Consider a simple mass-spring system with unit mass and nonlinear compliance as $\ddot{q} + F_c(q) = F_a$, where $F_c(q)q \geq 0$. In this simple dynamical system, the "natural" frequency of oscillations[3] (ω) is a function of their amplitude (A) as follows [35]:

$$\omega(A) = \frac{2\pi}{T(A)};\ T(A) = 2\sqrt{2}\int_0^A \frac{\mathrm{d}y}{\sqrt{\int_y^A f(z)\mathrm{d}z}}. \tag{13}$$

This equation proves that even in this simple dynamical system, the frequency of oscillations is a function of amplitude. Now consider an exemplary polynomial compliance profile as $F_c(q) = k|q|^{2\zeta-1}\mathrm{sign}(q)$, where $\mathrm{sign}(q \geq 0) = 1, \mathrm{sign}(q < 0) = -1, k > 0$, and $\zeta \geq 0.5$; the "natural" frequency is computed as follows:

$$\omega_{2\zeta-1}(A) = \alpha_{2\zeta-1}A^{\zeta-1};\ \alpha_{2\zeta-1} = \frac{\pi\sqrt{k}}{2\sqrt{2}\beta_{2\zeta-1}} > 0,\ \beta_{2\zeta-1} = \int_0^1 \frac{\mathrm{d}t}{\sqrt{1-t^{2\zeta}}} \tag{14}$$

In this equation, if $\zeta = 1$ (linear compliance; i.e., $F_c(q) = Kq$), the frequency is independent of the amplitude; $\omega_1(A) = \sqrt{k}$. And, if $\zeta = 2$ (cubic compliance; i.e., $F_c(q) = Kq^3$), the frequency is a linear function of amplitude; $\omega_3(A) = \alpha_3 A$. Therefore, based on Equation (13), any compliance profile except linear compliance leads to coupling between the frequency and amplitude of oscillations. □

We can utilize this property for nonlinear compliance design to improve both energy efficiency and control robustness over a set of m motions whose frequency and amplitude are coupled. Accordingly, we propose the following cost function as a metric for gait optimality, where w_i, F_{a_i}, and T_i are the corresponding weight, controller applied force, and the period of the i^{th} motion; using w_i, we can put more importance on some specific motions.

$$J_O = \sum_{i=1}^{m} w_i\int_{T_i} F_{a_i}^2\mathrm{d}t. \tag{15}$$

To compute the optimal compliance coefficients, we replace $\boldsymbol{F}_a = \boldsymbol{K}^{\mathrm{T}}\boldsymbol{\Phi} + \boldsymbol{F}_r$, calculate the partial derivative of J_O with respect to K, and compute K_O that minimizes J_O as follows:

$$K_O = -\boldsymbol{\Lambda}_O^{-1}\sum_{i=1}^{m} w_i\int_{T_i}\boldsymbol{F}_{r_i}\boldsymbol{\Phi}_i\mathrm{d}t,\quad \boldsymbol{\Lambda}_O = \sum_{i=1}^{m} w_i\int_{T_i}\boldsymbol{\Phi}_i^{\mathrm{T}}\boldsymbol{\Phi}_i\mathrm{d}t,\ \boldsymbol{\Lambda}_O \in \mathbb{R}^{m\times m}. \tag{16}$$

It is important to note that, considering Definition 1, $\boldsymbol{\Lambda}_R, \boldsymbol{\Lambda}_E$, and $\boldsymbol{\Lambda}_O$ are positive definite matrices and invertible.

To use this equation, the basis functions should be selected according to the FAC type using Equation (13). For instance, if the coupling is linear, based on Equation (14), a cubic basis function (e.g., $f(q) = Kq^3$) is a proper choice. Nevertheless, the nonlinear dynamics of the robot are also a main contributor that should be considered for selecting a proper set of basis functions.

3 | Simulation Results

To study the efficacy of the presented mathematics, in this section, we apply the proposed methods of parallel compliance design to a diverse set of robotic systems performing cyclic tasks; see Figure 3. We start the simulations with a 2-DOF robotic manipulator performing cyclic tasks in two different scenarios: (1) a single cyclic task and (2) a set of cyclic tasks

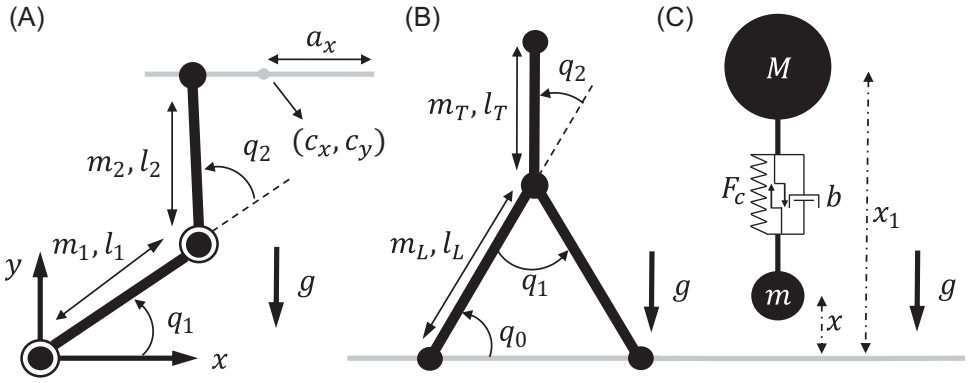

FIGURE 3 | The schematics of simulation models. (A) A 2-link manipulator performing a cyclic task with links' length and mass as $l_1 = l_2 = 1$ m and $m_1 = m_2 = 1$ kg. (B) A simple 3-DOF bipedal walker model performing symmetric gaits; i.e., $q_1 = -2q_0$ and $q_2 = \pi/2 - q_0$. In this model, the ankle (zero) joint does not have an actuator, and the hip (first) and trunk (second) joints are actuated. The robot links' length and mass are $l_L = 2$ m, $l_T = 1$ m, $m_L = 2$ kg, and $m_T = 3$ kg. (C) A simple hopper model performing hopping cycles. Due to the small mass ($m_2 \neq 0$), this model experiences sticking impact at the contact moments. The model's masses are $M = 1$ kg and $m = 0.1$ kg. In this model, the actuator is prismatic, and the damping coefficient is $b = 5$ Ns/m. In all three models, the compliance is in parallel configuration relative to the actuator and is left to be designed, and the gravity acceleration is set to $g = 9.81$ m/s^2.

with a linearly increasing FAC. To further investigate the FAC-based nonlinear compliance design in legged locomotion, we consider two more scenarios: (3) a 3-DOF bipedal robot performing gait cycles with a fixed frequency and (4) a hopper model with sticking-impact at the contact point performing hopping cycles with a nonlinear decreasing FAC.

In the first three scenarios (1–3), we compare the robot performance in terms of total energy consumption, applied force, and tracking error in four different conditions: (1) "*no compliant*," (2) "*linear compliance*," (3) "*piecewise linear compliance*," and (4) "*nonlinear compliance*." Here, "*piecewise linear compliance*" is considered a candidate for the estimation of "*nonlinear compliance*" with pieces of linear compliance. The basis functions for compliant conditions are selected as follows: "*linear compliance*"; $\boldsymbol{\Phi}_l = [1; q]$, "*nonlinear compliance*"; $\boldsymbol{\Phi}_n = [1; q; q^3]$, and "*piecewise linear compliance*"; $\boldsymbol{\Phi}_p = [1;(q-d)u(q-d);(q-d)u(d-q)]$ for the manipulator and $\boldsymbol{\Phi}_p = [1; q; (q-d)u(q-d); (q+d)u(-d-q)]$ for the 3-DOF biped, where 1 represents precompression, $u(x)$ is a step function such that $u(x \geq 0) = 1$ and $u(x < 0) = 0$, and d is the breakpoint in the piecewise linear profile, which is a design parameter and should be set based on the force-position profile at the corresponding joint. In manipulator simulations, d is set to $-32°$ and 80° for the first and second joints, respectively. In the 3-DOF bipedal model, d is set to 20° and 10° for the first and second controllable joints, respectively. In the hopper scenario (4), we compare the designed nonlinear compliance based on Equation (14) and linear compliance in terms of actuator applied force and controller tracking error in three different conditions: (1) "*no compliant*," (2) "*linear compliance*," and (3) "*nonlinear compliance*."

In manipulator simulations (1,2), the controller is a simple PD with fixed gains; first (second) joint PD gains are $K_p = 1000$ ($K_p = 1000$) and $K_d = 100$ ($K_d = 50$). The task is to move the end effector on $x = c_x + a_x \cos(\omega t)$ and $y = c_y$. In the 3-DOF bipedal model (3), the ankle (q_0) is passive (without an actuator); consequently, we employed the hybrid zero dynamics (HZD) controller to perform the walking cycles [36], where the trunk is always orthogonal relative to the horizontal (x), and the walking kinematic is symmetric; that is, $q_1 = -2q_0$ and $q_2 = \pi/2 - q_0$. In hopper simulations (4), the controller is a simple PD with $K_p = 10\,000$ and $K_d = 100$, and the task is to perform symmetric hopping trajectories at different heights of hop. In all simulations and all conditions, the robot initial condition (joint position and speed) is set on the desired trajectory; that is, the initial tracking error and its derivative are zero.

3.1 | Manipulator—Energy Efficiency and Robustness

In this scenario, we set $a_x = 0.4$ m and $\omega = 5$ rad/s to have a single cyclic task. To attain energy efficiency and control robustness on a single cyclic task, the optimal compliance is computed using Equation (10). For this simulation, the optimal compliance coefficients in "*linear*," "*piecewise linear*," and "*nonlinear*" conditions are computed as $\boldsymbol{K}_{l1} = [-7.9; 8.6]$, $\boldsymbol{K}_{l2} = [-14.2; 7.2]$, $\boldsymbol{K}_{p1} = [-15.6; 57.1; -3.4]$, $\boldsymbol{K}_{p2} = [-5.5; 9.6; -1.0]$, $\boldsymbol{K}_{n1} = [18.1; 71.3; -45.3]$, and $\boldsymbol{K}_{n2} = [-3.0; -3.8; 1.3]$. The overall simulation results are presented in Table 1. In addition, the tracking error, applied force, and force-position profiles for both joints are illustrated in Figure 4; the results are presented in steady state for one period of motion.

According to Figure 4A,D, compared to the "*no compliant*" condition, "*linear compliance*" leads to an 88% (80%) RMS applied force reduction at the first (second) joint, which results in an 87% total energy consumption reduction; see Table 1. Moreover, compared to "*linear compliance*," "*piecewise linear compliance*," and "*nonlinear compliance*" lead to 52% (64%) and 70% (76%) RMS applied force reduction at the first (second) joint, which yields 59% and 73% total energy consumption reductions, respectively; see Table 1.

According to Figure 4B,E, compared to the "*no compliant*" condition, "*linear compliance*" leads to 88% (82%) RMS tracking error reduction at the first (second) joint. And, compared to "*linear compliance*," "*piecewise linear compliance*," and "*nonlinear*

TABLE 1 | Simulation results for a specific cyclic task in a 2-DOF Manipulator. This table compares the "*no compliant*," "*linear compliance*," "*piecewise linear compliance*," and "*nonlinear compliance*" conditions in terms of RMS applied force, RMS tracking error, and total energy consumption. Compared to the "*no compliant*" condition, "*linear compliance*" reduces RMS applied force, RMS tracking error, and total energy consumption by at least 80%. Furthermore, both "*piecewise linear compliance*" and "*nonlinear compliance*" reduce these metrics by at least 50% compared to "*linear compliance*."

	Joint	Dimension	No compliant	Linear	Piecewise linear	Nonlinear
RMS applied force	First	[Nm]	14.02	1.65	0.79	0.49
	Second	[Nm]	3.64	0.71	0.25	0.17
RMS tracking error	First	[rad] × 1000	11.96	1.40	0.61	0.43
	Second	[rad] × 1000	7.27	1.32	0.56	0.33
Energy consumption	Total	[J]	20.08	2.64	1.09	0.72

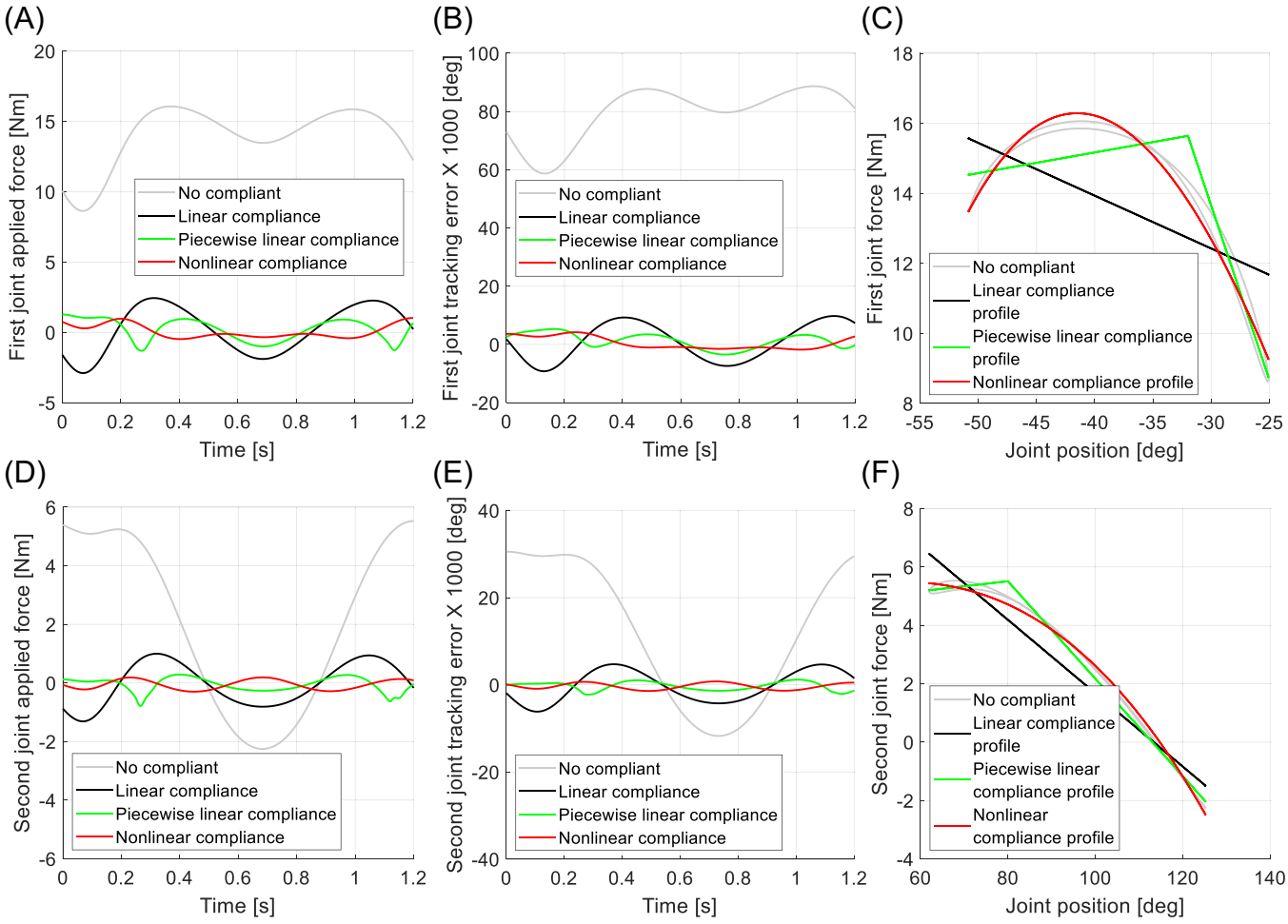

FIGURE 4 | Simulation results for a specific cyclic task in a 2-DOF manipulator. (A, D) Illustrate one period of controller applied force in the first and second joints, and (B, E) show one period of controller tracking error in the first and second joints. (C, F) Present the force-position profile of the controller in the "*no compliant*" condition, and the optimal compliance applied force in "*linear*," "*piecewise linear*," and "*nonlinear*" conditions for the first and second joints. All profiles are presented in steady state. Based on the illustrated results in (C, F), "*nonlinear compliance*" can properly estimate the force profile in the first and second joints, which yields a drastic reduction in both applied force (A, D) and tracking error (B, E) compared to both "*no compliant*" and "*linear compliance*" conditions. Also, the results indicate similar performance for "*nonlinear compliance*" and "*piecewise linear compliance*."

compliance" lead to 56% (58%) and 69% (75%) RMS tracking error reduction; see Table 1. Interestingly, in all conditions, the optimal compliance leads to a similar amount of applied force and tracking error reductions, which confirms our presented proof in Section 2.2.

Figure 4C,F illustrates the force-position profile of the applied force in the "*no compliant*" condition and the optimal force-position profile of "*linear compliance*," "*piecewise linear compliance*," and "*nonlinear compliance*." Clearly, "*piecewise linear compliance*" and "*nonlinear compliance*" significantly compensate for a main portion of the applied force in the "*no compliant*" condition, indicating a high level of energy consumption reduction, which modifies the natural dynamics of the system such that the control performance is improved and consequently the tracking error is also reduced.

3.2 | Manipulator—Gait Optimality

In this scenario, to have a linear FAC, we set $a_x = 0.4A$ m and $\omega = 5A$ rad/s, where A is the amplitude scaling factor and changes from $A = 1$ to $A = 1.5$ with a step of $\Delta A = 0.1$. To attain energy efficiency and control robustness over the set of motions, the optimal compliance coefficients are computed using Equation (16) with $w_i = 1$. For this simulation, the optimal compliance coefficients in "*linear*," "*piecewise linear*," and "*nonlinear*" conditions are computed as $\boldsymbol{K}_{l1} = [5.1; 28.2]$, $\boldsymbol{K}_{l2} = [-16.3; 9.0]$, $\boldsymbol{K}_{p1} = [-20.7; 106.7; -11.8]$, $\boldsymbol{K}_{p2} = [-7.7; 15.5; -4.4]$, $\boldsymbol{K}_{n1} = [43.2; 132.1; -82.5]$, and $\boldsymbol{K}_{n2} = [1.2; -9.6; 2.3]$. The simulation results are presented in Figure 5.

Figure 5A,B illustrates the force-position profiles of the applied force in the "*no compliant*" case and the optimal force-position profiles of "*linear compliance*," "*piecewise linear compliance*," and "*nonlinear compliance*" over the set of motions. Since the frequency and amplitude of the motions are coupled, the force-position profiles of the applied force have the same shape but scale by increasing the amplitude of motions. In this condition, "*linear compliance*" fails to properly compensate for these force profiles; however, "*nonlinear compliance*" can compensate for the average of the applied force profiles.

According to Figure 5D,E, except for $A = 1$, the "*linear compliance*" RMS applied force and RMS tracking error are always higher than "*piecewise linear compliance*" and "*nonlinear compliance*" for both joints, and the condition worsens in motions with higher amplitude. Finally, according to Figure 5F, the total energy consumption reduction of "*nonlinear compliance*" and "*piecewise linear compliance*" is mostly higher than the linear one.

3.3 | 3-DOF Bipedal Walker—Gait Optimality

In this scenario, the gait cycles are designed such that the stride length increases linearly from 35 cm to 170 cm, while the stride time is fixed at $t_s = 0.5$ s; that is, the frequency is constant and independent of the amplitude of motions ($\omega = 4\pi$ rad/s). To attain energy efficiency and control robustness over the gait cycles, the optimal compliance coefficients are computed using Equation (16)

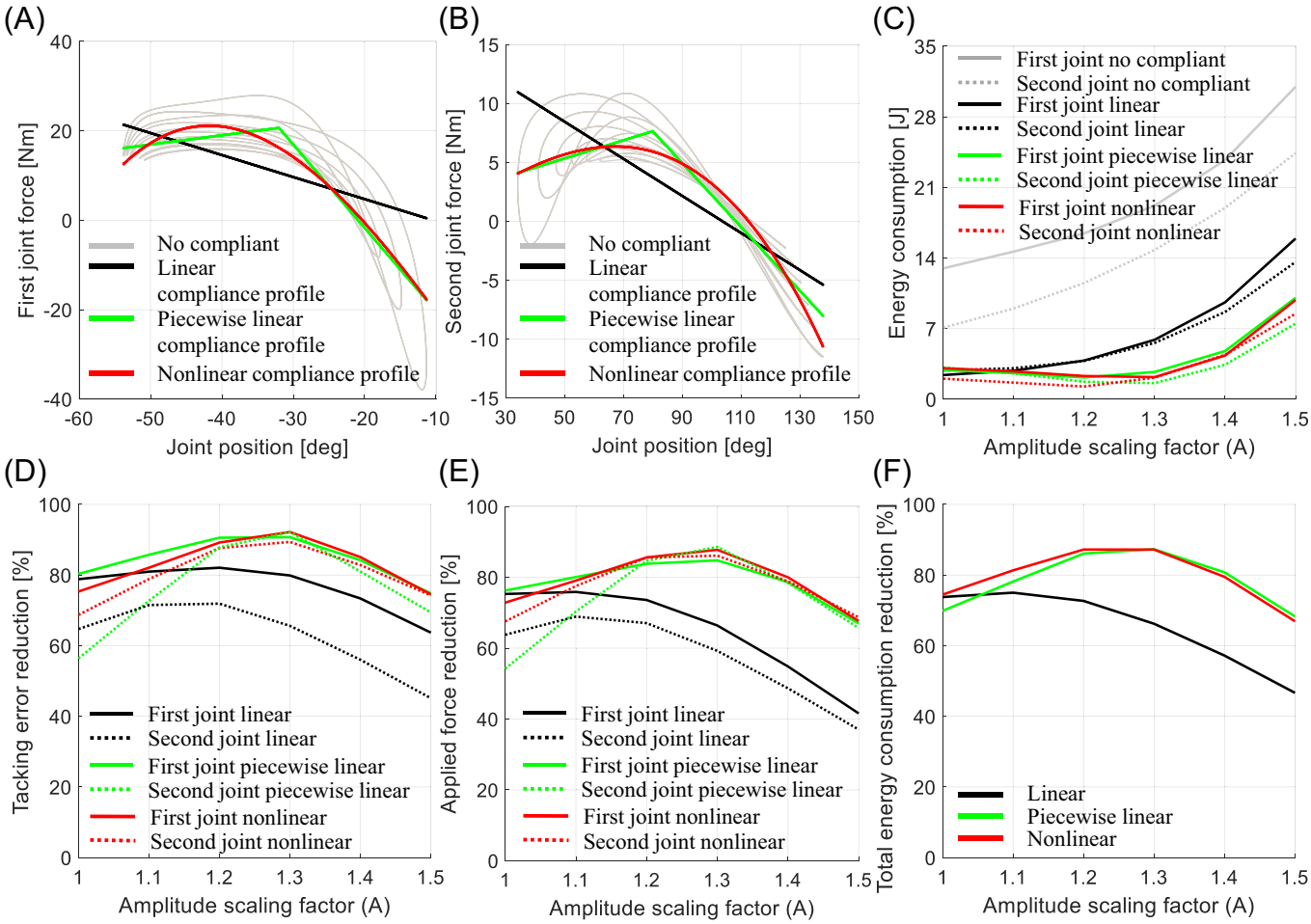

FIGURE 5 | Simulation results for gait optimality in a 2-DOF manipulator. (A, B) Present the force-position profile of the controller in the "*no compliant*" case, and the optimal compliance applied force in "*linear*," "*piecewise linear*," and "*nonlinear*" conditions for the first and second joints. (C) Shows the energy consumption of the robot for the first and second joints in "*no compliant*," "*linear compliance*," "*piecewise linear compliance*," and "*nonlinear compliance*." (D–F) Present the RMS tracking error, RMS applied force, and total energy consumption of the robot, respectively. Based on the illustrated results in (A, B), compared to "*linear compliance*," "*nonlinear compliance*" and "*piecewise linear compliance*" can properly estimate the average of force profiles over the set of motions in the first and second joints. This yields a higher reduction in tracking error (D), applied force (E), and total energy consumption (F) compared to "*linear compliance*."

with $w_i = 1$. In this simulation, the optimal compliances in "*linear*," "*piecewise linear*," and "*nonlinear*" conditions are designed using Equation (16) as $\boldsymbol{K}_{l1} = [0.0; -19.8]$, $\boldsymbol{K}_{l2} = [0.0; 11.6]$, $\boldsymbol{K}_{p1} = [0.0; -25.2; 18.1; 18.1]$, $\boldsymbol{K}_{p2} = [0.0; 14.8; -12.4; -12.4]$, $\boldsymbol{K}_{n1} = [0.0; -25.8; 19.2]$, and $\boldsymbol{K}_{n2} = [0.0; 15.1; -52.5]$. The simulation results are presented in Figure 6A–C, including the compliance and actuator force profiles and energy consumption reduction. Due to using a dynamic compensation controller (i.e., HZD), the perfect tracking condition (identically zero tracking error and its derivative) is attained for all conditions; hence, the tracking error is not reported in this simulation.

Figure 6A,B compares the force-position profile of the "*no compliant*," "*linear compliance*," "*piecewise linear compliance*," and "*nonlinear compliance*" conditions at the first (q_1) and second (q_2) controllable joints. As is clear, "*linear compliance*" can only compensate for the "*no compliant*" force in the lower set of motions (i.e., $|q_1| < 25°$ and $|q_2| < 12.5°$). Figure 6C shows the total energy consumption reduction compared to the no-compliant condition for different step lengths; clearly, "*piecewise linear compliance*" and "*nonlinear compliance*" have similar performance regarding energy consumption reduction; however, they are both better than the "*linear compliance*" condition.

Based on our mathematics presented in Section 2.3, for mass-spring systems, a fixed frequency leads to an identical optimal linear compliance regardless of the considered set of motions. However, due to the nonlinearity in bipedal robot dynamics, even a fixed frequency leads to a set of nonlinear applied force profiles that cannot be properly compensated by linear compliance.

3.4 | Hopper Model—Gait Optimality

In this scenario, due to the simplicity of the hopper dynamics, instead of optimizing the compliance profile, the compliance force

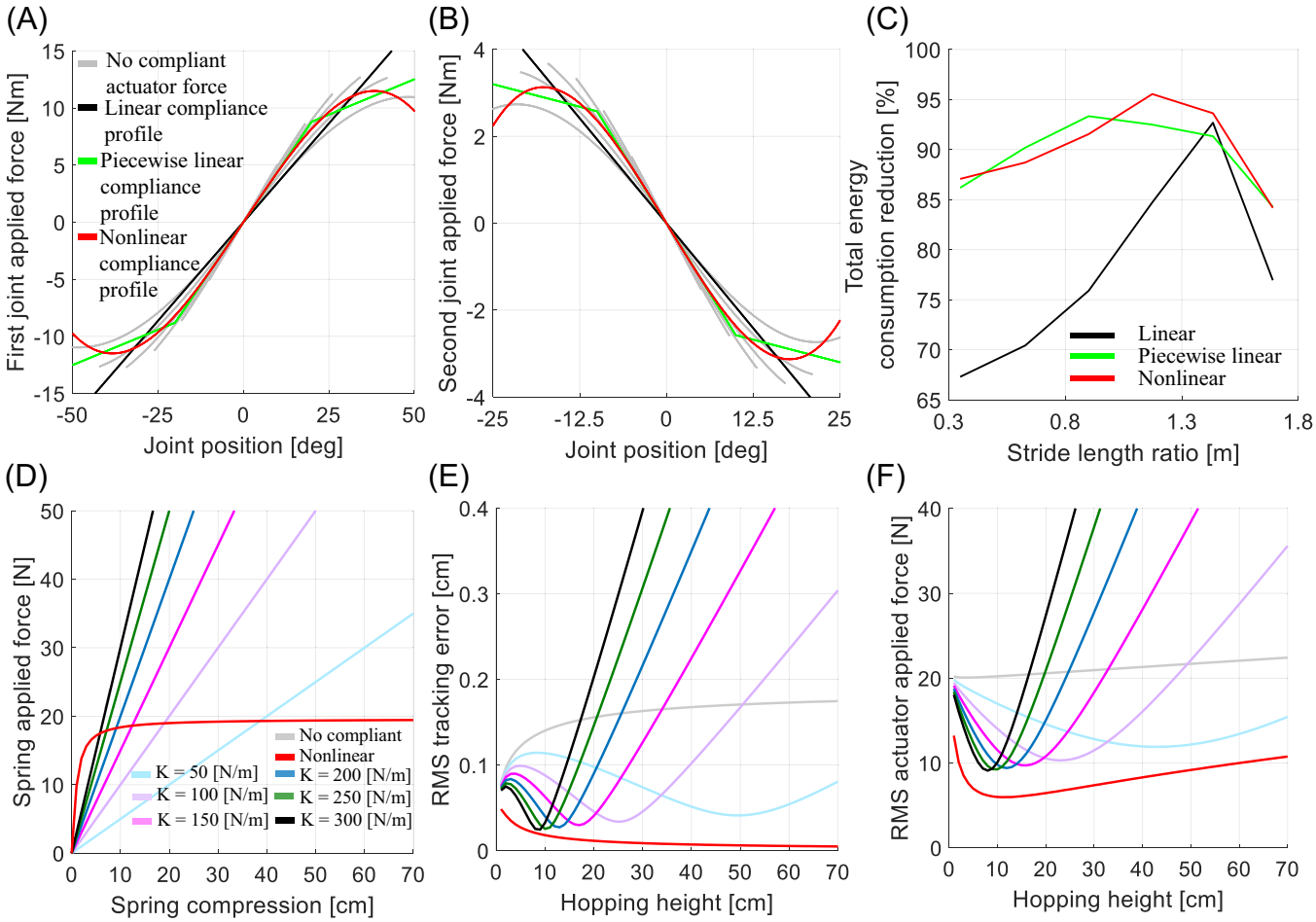

FIGURE 6 | Simulation results for gait optimality in 3-DOF bipedal walker and hopper models. (A–C) Are the simulation results for a 3-DOF bipedal walker with a fixed frequency. (A, B) Present the force-position profile of the controller in the "*no compliant*" case, and the optimal compliance force profiles in "*linear*," "*piecewise linear*," and "*nonlinear*" conditions for the first and second controllable joints (q_1, q_2). (C) Compares the total energy consumption reduction in "*linear compliance*," "*piecewise linear compliance*," and "*nonlinear compliance*" with respect to the "*no compliant*" condition. Based on the illustrated results in (A, B), Compared to "*linear compliance*," "*nonlinear compliance*" and "*piecewise linear compliance*" can properly estimate the average of force profiles over the set of motions in the first and second joints. This yields a higher reduction in total energy consumption (C) for the bipedal walker model simulation. (D–F) Are the simulation results for the hopping model. (D) Shows the "*linear*" and "*nonlinear*" compliance force profiles for hopper simulation. (E) and (F) Compare "*no compliant*," "*linear*," and "*nonlinear*" compliance conditions in terms of the RMS actuator applied force and RMS tracking error over one hopping cycle at different hopping heights. Based on (E, F), compared to all "*linear compliance*" profiles, the designed "*nonlinear compliance*" profile leads to a higher reductions in RMS tracking error (E) and RMS actuator applied force (F) for all hopping heights.

is computed analytically. The hopper system has hybrid dynamics, stance and flight. Neglecting the dynamics of the small mass (x_2), the dynamics of the large mass (x_1) during the flight and stance phases are $M\ddot{x}_1 + Mg = 0$ and $M\ddot{x}_1 + B_s\dot{x}_1 + F_c(x_1) + Mg = F_a$, respectively, where B_s is the damping coefficient. During the flight phase, the system has no control over the large mass trajectory, and the large mass has parabolic motion as $x_1(t) = -0.5gt^2 + v_0 t + d$, where d is the spring rest length, x_1 is the position of the large mass, $v_0 > 0$ is the flight initial velocity, and g is gravitational acceleration. To have symmetric hopping cycles, the flight trajectory should be flipped to design the stance trajectory as $x_1(t) = 0.5gt^2 - v_0 t + d$.

Considering the designed flight and stance trajectories, the period of one hopping cycle is twice the flight duration (t_f) as $T = 2t_f = 4v_0/g$. Using conservation of energy, the flight phase initial velocity is computed as a function of hopping height (amplitude; A) as $mgA = 0.5mv_0^2 \rightarrow v_0 = \sqrt{2Ag}$. Hence, the frequency of hopping can be computed as $\omega = 2\pi/T = \pi\sqrt{g}/(2\sqrt{2})A^{-0.5} \rightarrow \omega \propto A^{-0.5}$; the symmetric hopping has a nonlinearly decreasing FAC. Comparing this equation with Equation (14), we can conclude that $\zeta = 0.5, \beta_0 = 1, k = g$, the compliance force is $f = g\,\mathrm{sign}(x_1 - d)$, and consequently, the system dynamics should be written as $\ddot{x}_1 + g\,\mathrm{sign}(x_1 - d) = 0$. Comparing these dynamics with the hybrid dynamics of the hopper system indicates that the compliance in the hopper system should be designed as $F_c(h) = -2Mgu(h)$, where $h = d - x_1$ is the spring compression length. However, this compliance profile is discontinuous and cannot be implemented in practice. To resolve this issue, we approximate $-u(h)$ with a continuous function as $2/\pi \tan^{-1}(\Gamma h)u(h)$, where increasing $\Gamma > 0$ improves the approximation accuracy. Considering this approximation, the designed nonlinear compliance profile is $F_c(h) = 4gM/\pi \tan^{-1}(\Gamma h)u(-h)$, where in this simulation $M = 1\text{kg}$, $g = 9.81\ \text{m/s}^2$, and $\Gamma = 100$. Figure 6D illustrates the linear and nonlinear compliance force profiles as a function of spring compression during the stance phase.

Figure 6D–F present the hopping overall simulation results, where we compare the designed nonlinear compliance performance with a range of linear compliances with different coefficients; for all compliance profiles, the zero force is at zero compression ($h = 0$). Figure 6E,F compares "*no compliant*," "*linear compliance*," and "*nonlinear compliance*" in terms of the RMS actuator applied force and RMS tracking error over one hopping cycle at different hopping heights. Based on the results, for all '*linear compliance*' coefficients, the minimum of both RMS applied force and RMS tracking error is higher than the "*nonlinear compliance*" condition. This also indicates that, for a specific hopping height, "*linear compliance*" can be a good suboptimal solution. For instance, for 10 and 50 cm hopping heights, the best linear solutions are linear compliance with 250 and 50 N/m, respectively. However, to have energy efficiency over a range of hopping heights, having "*nonlinear compliance*" is a must.

4 | Conclusion and Discussion

In this article, we presented a systematic method to design nonlinear parallel compliance to achieve energy efficiency, control robustness, and gait optimality. Moreover, we analytically proved the superiority of nonlinear compliance over linear compliance in terms of energy consumption reduction, tracking error reduction, and gait optimality. The proposed method was evaluated using a diverse set of simulated robotic systems, including a two-link manipulator, a 3-DOF bipedal walker, and a hopper system. It was also observed that designing the compliance to improve control robustness leads to both tracking error and energy consumption minimization.

Based on the simulation results, it is concluded that having only linear compliance is beneficial to improve energy efficiency and control robustness compared to the no-compliant case. But, to attain a higher performance in terms of energy consumption and control robustness across a set of motions, nonlinear compliance is required. It is investigated that, due to coupling between the frequency and amplitude in nonlinear compliances, only the nonlinear compliances have the potential to improve gait optimality. In addition, comparing the results of piecewise linear and nonlinear compliance, it is concluded that piecewise linear compliance is a practical solution to realize different types of nonlinear compliance profiles using a few linear compliances.

Based on the proposed results, the presented method for nonlinear compliance design can enhance the robot controller performance. Minimizing the tracking error indicates that the proposed method can improve the closed-loop control performance such that a weak controller or actuator can be utilized in the robotic system with nonlinear parallel compliance. In addition, minimizing the robustness cost function not only minimizes the reliance on the controller performance, but also minimizes the actuator's maximum applied force. This potentially leads to using smaller actuators and prevents the control command (actuator force) saturation which is one of the most common instability reasons in practice.

The main limitation of this study is the lack of experimental implementation on a robotic system, which is considered as our future work. Nevertheless, focusing on the simulated robotic models provides us with a general formalism to compare the main advantages of nonlinear compliance over the linear one not only in robotic systems but also in other systems benefiting nonlinear compliances; for example, animal biomechanics. The animals attain stability, efficiency, safety, robustness, adaptability, and so on using their neuromuscular system (i.e., muscles which are also modeled as compliance) rather than their rigid skeleton. The analytical analysis and robotic modeling such as [37] are methods to address the biological pieces of evidence on gait quality and gait optimality attained by a compliant body. Inspired by nature, in this study, we presented a mathematical framework to design nonlinear compliance and improve the robotic system performance in cyclic tasks. The following subsections discuss some other aspects of nonlinear parallel compliance design, possible extensions, and future work.

4.1 | Gait Optimality and Pattern Generator

In many robotic applications, the system has an adaptive pattern generator. To maximally utilize the FAC feature of nonlinear compliance, the FAC of the selected nonlinear compliance can be imposed in the pattern generator dynamics. In this case, instead of frequency-adaptive oscillators [38],

nonlinear adaptive oscillators [39] with selectable nonlinear basis functions are recommended.

4.2 | Basis Function Selection

The efficacy of nonlinear compliance is highly tied to the proper selection of basis functions. In this case, prior knowledge about the force-position profile at the targeted joint [21] and the frequency-amplitude coupling type of the motions are essential. Nevertheless, to design nonlinear compliance with better performance compared to linear compliance, instead of the selected nonlinear basis function, it is required to have a unit and a linear basis function in the set of bases. Having the suggested bases guarantees that the baseline performance of the designed nonlinear compliance is better than the linear one; see Section 2.1 for more details.

4.3 | Bi-Articular Compliance

Due to the coupling terms in nonlinear dynamics, such as Coriolis and gravity forces, in many cases, the applied force cannot be properly compensated by compliance that applies force as a function of the targeted joint position; that is, mono-articular compliance. Biology resolves this problem using compliances (muscles) that apply force to two adjacent joints; that is, bi-articular muscles [40–42]. From an analytical view, bi-articular compliance has more potential to reduce energy consumption and improve control robustness [43]. To design a bi-articular compliance profile, it is sufficient to consider the basis functions as a summation of the targeted and adjacent joint angles. In addition, using bi-articular compliance.

4.4 | Estimation of the Applied Force

To optimize the compliance profile, the required force over the desired motion should be known, which seems challenging. The solutions to estimate the required torque are using (1) a simulated model of the robot controlled over the desired trajectory and (2) the recorded DC-motor current in an experimental setup [44].

4.5 | Variable Compliance Versus Gait Optimality

The optimal nonlinear compliance profile is a function of the reference trajectory, which differs in different conditions. A solution to deal with changes in the optimal compliance profile is to update the compliance profile using compliance adaptation rules [45–47] and adaptable mechanisms [48–50]; however, designing adaptive nonlinear compliance is complex and expensive. Besides, frequent variations of the compliance profile increase the costs of compliance adaptation and make the overall system inefficient. Hence, gait optimality is an alternative solution for cases where adaptation is not cost-efficient and we have a certain FAC; that is, we have a certain gait.

Acknowledgments

The authors would like to thank the University of Tehran for providing support with this study. Special thanks go to Amir Sarabi for his comments on the first draft of this paper.

Conflicts of Interest

The authors declare no conflicts of interest.

Data Availability Statement

The authors have nothing to report.

Endnotes

[1] In the rest of the paper, for the sake of simplicity and without loss of generality, we focus on one arbitrary joint of the robot, and accordingly, we may forbear specifying the joint index. Hence, we refer to the jth joint's desired position, real position, applied force, parallel compliance force, parallel compliance function, and tracking error as $q \in \mathbb{R}$, $q_r \in \mathbb{R}$, $F_a \in \mathbb{R}$, $F_c \in \mathbb{R}$, and $e \in \mathbb{R}$, respectively.

[2] Any pair of linearly independent functions can be represented as an orthogonal pair; i.e., the *Gram-Schmidt* orthogonalization process [33, 491].

[3] The natural frequency is the frequency of unforced periodic motions; i.e., $F_a \equiv 0$.

References

1. A. J. Ijspeert, "Central Pattern Generators for Locomotion Control in Animals and Robots: A Review," *Neural Networks* 21, no. 4 (2008): 642–653.

2. Y. Mezouar and F. Chaumette, "Path Planning for Robust Image-Based Control," *IEEE Transactions on Robotics and Automation* 18, no. 4 (2002): 534–549.

3. S. Collins, A. Ruina, R. Tedrake, and M. Wisse, "Efficient Bipedal Robots Based on Passive-Dynamic Walkers," *Science* 307, no. 5712 (2005): 1082–1085.

4. R. M. Alexander, "Three Uses for Springs in Legged Locomotion," *International Journal of Robotics Research* 9, no. 2 (1990): 53–61.

5. S. Oh and K. Kong, "High-Precision Robust Force Control of a Series Elastic Actuator," *IEEE/ASME Transactions on Mechatronics* 22, no. 1 (2016): 71–80.

6. T. D. Niehues, P. Rao, and A. D. Deshpande, "Compliance in Parallel to Actuators for Improving Stability of Robotic Hands During Grasping and Manipulation," *International Journal of Robotics Research* 34, no. 3 (2015): 256–269.

7. M. A. Sharbafi, C. Rode, S. Kurowski, et al., "A New Biarticular Actuator Design Facilitates Control of Leg Function in Biobiped3," *Bioinspiration & Biomimetics* 11, no. 4 (2016): 046003.

8. G. Tonietti, R. Schiavi, and A. Bicchi, "Design and Control of a Variable Stiffness Actuator for Safe and Fast Physical Human/Robot Interaction," in Proceedings of the 2005 IEEE International Conference on Robotics and Automation (IEEE, 2005), 526–531.

9. A. Jafari, N. G. Tsagarakis, and D. G. Caldwell, "A Novel Intrinsically Energy Efficient Actuator With Adjustable Stiffness (Awas)," *IEEE/ASME Transactions on Mechatronics* 18, no. 1 (2011): 355–365.

10. N. Schmit and M. Okada, "Optimal Design of Nonlinear Springs in Robot Mechanism: Simultaneous Design of Trajectory and Spring Force Profiles," *Advanced Robotics* 27, no. 1 (2013): 33–46.

11. H. J. Bidgoly, M. N. Ahmadabadi, and M. R. Zakerzadeh, " Design and Modeling of a Compact Rotational Nonlinear Spring," in 2016 IEEE/RSJ International Conference on Intelligent Robots and Systems (IROS) (IEEE, 2016), 4356–4361.

12. M. A. Shahri, O. Mohseni, H. J. Bidgoly, and M. N. Ahmadabadi, "Profile Design of Parallel Rotary Compliance for Energy Efficiency in Cyclic Tasks," *IEEE/ASME Transactions on Mechatronics* 25, no. 1 (2019): 142–151.

13. M. A. Sharbafi, M. J. Yazdanpanah, M. N. Ahmadabadi, and A. Seyfarth, "Parallel Compliance Design for Increasing Robustness and

Efficiency in Legged Locomotion-Theoretical Background and Applications," *IEEE/ASME Transactions on Mechatronics* 26, no. 1 (2020): 335–346.

14. R. Chen, R. Song, Z. Zhang, et al., "Bio-Inspired Shape-Adaptive Soft Robotic Grippers Augmented With Electroadhesion Functionality," *Soft Robotics* 6, no. 6 (2019): 701–712.

15. L. Ventura, M. Lorenzini, W. Kim, and A. Ajoudani, "A Flexible Robotics-Inspired Computational Model of Compressive Loading on the Human Spine," *IEEE Robotics and Automation Letters* 6, no. 4 (2021): 8229–8236.

16. Z. Bing, A. Rohregger, F. Walter, et al., "Lateral Flexion of a Compliant Spine Improves Motor Performance in a Bioinspired Mouse Robot," *Science Robotics* 8, no. 85 (2023): eadg7165.

17. M. Grimmer, M. Eslamy, S. Gliech, and A. Seyfarth, " A Comparison of Parallel-and Series Elastic Elements in an Actuator for Mimicking Human Ankle Joint in Walking and Running," in 2012 IEEE International Conference on Robotics and Automation (IEEE, 2012), 2463–2470.

18. N. L. Tagliamonte, F. Sergi, D. Accoto, G. Carpino, and E. Guglielmelli, "Double Actuation Architectures for Rendering Variable Impedance in Compliant Robots: A Review," *Mechatronics* 22, no. 8 (2012): 1187–1203.

19. B. Vanderborght, A. Albu-Schäffer, A. Bicchi, et al., "Variable Impedance Actuators: A Review," *Robotics and Autonomous Systems* 61, no. 12 (2013): 1601–1614.

20. T. Verstraten, P. Beckerle, R. Furnémont, G. Mathijssen, B. Vanderborght, and D. Lefeber, "Series and Parallel Elastic Actuation: Impact of Natural Dynamics on Power and Energy Consumption," *Mechanism and Machine Theory* 102 (2016): 232–246.

21. M. Khoramshahi, A. Parsa, A. Ijspeert, and M. N. Ahmadabadi, "Natural Dynamics Modification for Energy Efficiency: A Data-driven Parallel Compliance Design Method," in 2014 IEEE International Conference on Robotics and Automation (ICRA) (IEEE, 2014), 2412–2417.

22. O. Bey and M. Chemachema, "Decentralized Event-Triggered Output Feedback Adaptive Neural Network Control for a Class of Mimo Uncertain Strict-Feedback Nonlinear Systems With Input Saturation," *International Journal of Adaptive Control and Signal Processing* 38, no. 4 (2024): 1420–1441.

23. R. Nasiri, A. Zare, O. Mohseni, M. J. Yazdanpanah, and M. N. Ahmadabadi, "Concurrent Design of Controller and Passive Elements for Robots With Impulsive Actuation Systems," *Control Engineering Practice* 86 (2019): 166–174.

24. Z. Ju, K. Wei, L. Jin, and Y. Xu, "Investigating Stability Outcomes Across Diverse Gait Patterns in Quadruped Robots: A Comparative Analysis," *IEEE Robotics and Automation Letters* 9, no. 1 (2023): 795–802.

25. A. Cully, J. Clune, D. Tarapore, and J. B. Mouret, "Robots That Can Adapt Like Animals," *Nature* 521, no. 7553 (2015): 503–507.

26. J. P. Gasc, "Comparative Aspects of Gait, Scaling and Mechanics in Mammals," *Comparative Biochemistry and Physiology Part A: Molecular & Integrative Physiology* 131, no. 1 (2001): 121–133.

27. R. M. Alexander, *Principles of Animal Locomotion* (Princeton University Press, 2003).

28. E. L. Shepard, R. P. Wilson, W. G. Rees, E. Grundy, S. A. Lambertucci, and S. B. Vosper, "Energy Landscapes Shape Animal Movement Ecology," *American Naturalist* 182, no. 3 (2013): 298–312.

29. N. C. Heglund, C. R. Taylor, and T. A. McMahon, "Scaling Stride Frequency and Gait to Animal Size: Mice to Horses," *Science* 186, no. 4169 (1974): 1112–1113.

30. N. C. Heglund and C. R. Taylor, "Speed, Stride Frequency and Energy Cost Per Stride: How Do They Change With Body Size and Gait?," *Journal of Experimental Biology* 138, no. 1 (1988): 301–318.

31. K. Strang and K. Steudel, "Explaining the Scaling of Transport Costs: the Role of Stride Frequency and Stride Length," *Journal of Zoology* 221, no. 3 (1990): 343–358.

32. Freep!k Graphic Vectors, 2024, https://www.freepik.com/vectors/graphics.

33. G. A. Korn and T. M. Korn, *Mathematical Handbook for Scientists and Engineers: Definitions, Theorems, and Formulas for Reference and Review* (Courier Corporation, 2000).

34. K. Zhou and J. C. Doyle, *Essentials of Robust Control* (Prentice Hall, 1998), 104.

35. H. K. Khalil, *Nonlinear Systems* (Prentice hall, 2002).

36. E. R. Westervelt, J. W. Grizzle, and D. E. Koditschek, "Hybrid Zero Dynamics of Planar Biped Walkers," *IEEE Transactions on Automatic Control* 48, no. 1 (2003): 42–56.

37. H. Geyer, A. Seyfarth, and R. Blickhan, "Compliant Leg Behaviour Explains Basic Dynamics of Walking and Running," *Proceedings of the Royal Society B: Biological Sciences* 273, no. 1603 (2006): 2861–2867.

38. M. Khoramshahi, R. Nasiri, M. Shushtari, A. J. Ijspeert, and M. N. Ahmadabadi, "Adaptive Natural Oscillator to Exploit Natural Dynamics for Energy Efficiency," *Robotics and Autonomous Systems* 97 (2017): 51–60.

39. R. Nasiri, M. Khoramshahi, and M. N. Ahmadabadi, "Design of a Nonlinear Adaptive Natural Oscillator: Towards Natural Dynamics Exploitation in Cyclic Tasks," in 2016 IEEE/RSJ International Conference on Intelligent Robots and Systems (IROS) (IEEE, 2016), 3653–3658.

40. G. J. van Ingen Schenau, M. F. Bobbert, and R. H. Rozendal, "The Unique Action of Bi-Articular Muscles in Complex Movements," *Journal of Anatomy* 155 (1987): 1.

41. G. J. V. I. Schenau, "From Rotation to Translation: Constraints on Multi-Joint Movements and the Unique Action of Bi-Articular Muscles," *Human Movement Science* 8, no. 4 (1989): 301–337.

42. R. Jacobs, M. F. Bobbert, and G. J. van Ingen Schenau, "Mechanical Output From Individual Muscles During Explosive Leg Extensions: The Role of Biarticular Muscles," *Journal of Biomechanics* 29, no. 4 (1996): 513–523.

43. H. J. Bidgoly, A. Parsa, M. J. Yazdanpanah, and M. N. Ahmadabadi, "Benefiting From Kinematic Redundancy Alongside Mono-and Biarticular Parallel Compliances for Energy Efficiency in Cyclic Tasks," *IEEE Transactions on Robotics* 33, no. 5 (2017): 1088–1102.

44. A. Wahrburg, J. Bös, K. D. Listmann, F. Dai, B. Matthias, and H. Ding, "Motor-Current-Based Estimation of Cartesian Contact Forces and Torques for Robotic Manipulators and Its Application to Force Control," *IEEE Transactions on Automation Science and Engineering* 15, no. 2 (2017): 879–886.

45. M. Uemura, S. Kawamura, H. Hirai, and F. Miyazaki, "Iterative Motion Learning With Stiffness Adaptation for Multi-joint Robots," in 2014 IEEE International Conference on Robotics and Biomimetics (ROBIO 2014) (IEEE, 2014), 1088–1093.

46. R. Nasiri, M. Khoramshahi, M. Shushtari, and M. N. Ahmadabadi, "Adaptation in Variable Parallel Compliance: Towards Energy Efficiency in Cyclic Tasks," *IEEE/ASME Transactions on Mechatronics* 22, no. 2 (2016): 1059–1070.

47. O. Mohseni, M. A. Shahri, A. Davoodi, and M. N. Ahmadabadi, "Adaptation in a Variable Parallel Elastic Actuator for Rotary Mechanisms Towards Energy Efficiency," *Robotics and Autonomous Systems* 143 (2021): 103815.

48. B. Vanderborght, R. Van Ham, D. Lefeber, T. G. Sugar, and K. W. Hollander, "Comparison of Mechanical Design and Energy Consumption of Adaptable, Passive-Compliant Actuators," *International Journal of Robotics Research* 28, no. 1 (2009): 90–103.

49. A. Jafari, N. G. Tsagarakis, and D. G. Caldwell, "AwAS-II: A New Actuator With Adjustable Stiffness Based on the Novel Principle of Adaptable Pivot Point and Variable Lever Ratio," in 2011 IEEE International Conference on Robotics and Automation (IEEE, 2011), 4638–4643.

50. R. Nasiri, A. Ahmadi, and M. N. Ahmadabadi, "Realization of Nonlinear Adaptive Compliance: Towards Energy Efficiency in Cyclic Tasks," in 2019 7th International Conference on Robotics and Mechatronics (ICRoM) (IEEE, 2019), 175–180.